8

Realizing Efficient Wireless Power Transfer in the Near-Field Region Using Electrically Small Antennas

Ick-Jae Yoon and Hao Ling
Dept. of Electrical and Computer Engineering,
The University of Texas at Austin,
USA

1. Introduction

In the early 1900's, Tesla carried out his experiment on power transmission over long distances by radio waves (Tesla, 1914). He built a giant coil (200-ft mast and 3-ft-diameter copper ball positioned at the top) resonating at 150 kHz and fed it with 300 kW of low frequency power. However, there is no clear record of how much of this power was radiated into space and whether any significant amount of it was collected at a distant point. Over the years, wireless power delivery systems have been conceived, tried and tested by many (Brown, 1984; Glaser, 1968; McSpadden et al., 1996; Shinohara & Matsumoto, 1998; Strassner & Chang, 2002; Mickle, et al., 2006; Conner, 2007). For very short ranges, the inductive coupling mechanism is commonly exploited. This is best exemplified by non-contact chargers and radio frequency identification (RFID) devices operating at 13 MHz (Finkenzeller, 2003). Such systems are limited to ranges that are less than the device size itself. For long distance wireless power delivery, directed radiation is required, which dictates the use of large aperture antennas. This line of thinking is best exemplified by NASA's effort to collect solar power on a single satellite station in space and relay the collected power via microwaves to power other satellites in orbit (Glaser, 1968). In addition to needing large antennas, this scheme requires uninterrupted line-of-sight propagation and a potentially complicated tracking system for mobile receivers.

In 2007, MIT physicist Soljačić and his group demonstrated the feasibility of efficient non-radiative wireless power transfer using two resonant loop antennas (Kurs et al., 2007). Since then, there has been much interest from the electromagnetics community to more closely study this phenomenon (Kim & Ling, 2007; Jing & Wang, 2008; Kim & Ling, 2008; Pan et al., 2009; Thomas et al., 2010; Jung and Lee, 2010; Cannon et al., 2009; Kurs et al., 2010; Casanova et al., 2009). It was found that when two antennas are very closely spaced, they are locked in a coupled mode resonance phenomenon. In this coupled mode region, the two antennas see each other's presence strongly, and very high power transfer efficiency (PTE) can be attained (see Fig. 1). The term magnetic resonance coupling is often used to describe this phenomenon, although such coupled mode resonance can exist in antenna systems dominated by either magnetic or electric coupling, as shown in (Kim & Ling, 2007). It was also found that to maximize the power transfer the antennas need to have low radiation loss

so that power is not lost to the radiation process. However, such a coupled mode region is very short when measured in terms of wavelength and attempts to design antennas to extend the distance over which such coupled mode phenomenon can be maintained have proven to be rather difficult (Kim & Ling, 2008). If the range can be extended, it could potentially benefit a number of applications including RFID (Fotopoulou & Flynn, 2007; Fotopoulou & Flynn, 2011; Sample & Smith, 2009; Bolomey et al., 2010; Yates et al., 2004), biomedical implants (Poon et al., 2010; RamRakhyani et al., 2011; Smith et al., 2007; Fotopoulou & Flynn, 2006), and electric car charging (Eom & Arai, 2009; Imura et al., 2009).

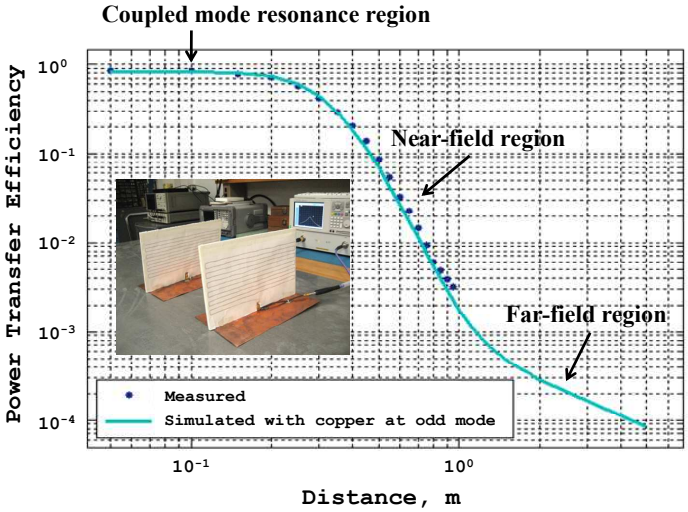

Fig. 1. Power transfer efficiency vs. distance between two electrically small meander antennas operating at 43MHz (Kim & Ling, 2007).

When the distance between the two antennas increases, the coupled mode resonance phenomenon disappears, and the antennas behave like traditional transmitting and receiving antennas in the near field (see Fig. 1). Beyond the coupled mode region, the PTE decreases rapidly as a function of distance. Nevertheless, sufficiently high PTE values might still be maintained for such coupling to be useful for power transfer. The physics beyond the coupled mode region is significantly easier to interpret. There have been works on the coupling properties of antennas in the near-field region, though the interest was not wireless power transfer. In the 1970's, theoretical and practical aspects of the spherical near-field antenna measurement were extensively studied at the Technical University of Denmark (Hansen, 1988). Yaghjian formulated a coupling equation between a transmitting and receiving antenna pair by the spherical wave expansion (Yaghjian, 1982). To more accurately estimate the coupling in the near-filed region, heuristic corrections to the far-field Friis formula were also attempted by adding higher order distance terms (Schantz, 2005) or by adding a gain reduction factor (Kim et al., 2010). Recently, a theoretical PTE bound for wireless power transfer in the near-field region was presented under the optimal load condition by Lee and Nam (Lee & Nam, 2010). They applied the spherical mode theory to study the coupling between two electrically small antennas in this region. It was found that

a 40% PTE value can be theoretically achieved at a distance of 0.26λ in the co-linear configuration of electric dipole antennas, while the same PTE value was obtained at 0.067λ based on the MIT experiment using two small resonant multi-turn coils under coupled mode operation (Kurs et al., 2007). It was also shown that high antenna radiation efficiency is needed to maximize the power transfer beyond the coupled mode region. This implies that existing knowledge on the design of highly efficient small antennas for far-field applications can be leveraged upon to achieve the upper PTE bound in the near-field region. The design of electrically small but highly efficient antennas is a research topic that has been well investigated in the past decade (Dobbins & Rogers, 2001; Choo & Ling, 2003; Best, 2004; Lim & Ling, 2006). Among the various small antenna designs, the most well known is the folded spherical helix (FSH) by Best (Best, 2004). In his design, four arms are wound helically along a spherical surface and the arms are connected at the top. Such design uses multiple folds to step up the radiation resistance. The reported size of kr is 0.38 (where k is the free-space wave number and r is the minimum size of the imaginary sphere enclosing the antenna). The FSH monopole antenna yields a low Q (32) and high radiation efficiency η (98.6%) despite its small size. The folded cylindrical helix (FCH) has also been investigated (Johnston & Haslett, 2005; Best, 2009; Best, 2009). Although it does not achieve as low a Q-factor as that of the FSH, it has a form factor that is easier to construct and handle.

While recent research on wireless power transfer has been mostly centered on the coupled mode phenomenon, we focus our attention in this chapter on the near-field region beyond the coupled mode resonance region. In particular, it will be shown that electrically small antennas can be designed to realize efficient wireless power transfer in the near field. This chapter is organized as follows. In Sec. 2, we show that the theoretical bound derived in (Lee & Nam, 2010) can be approached in practice by the use of two electrically small but highly efficient FCH dipoles. In Sec. 3, we discuss transmitter and receiver diversity as a means to extend the range or efficiency of the near-field power transfer. We derive the theoretical PTE bounds under transmitter diversity and receiver diversity and then achieve the bounds experimentally using actual FCH dipoles. In Sec. 4, we investigate electrically small, directive antennas as a means of increasing the range or power transfer efficiency in the near-field region. Sec. 5 presents conclusions and discusses future research directions.

2. Achieving power transfer bound using electrically small antennas

2.1 Theoretical bound for near-field power transfer and antenna design considerations

We will first review the theoretical results from (Lee & Nam, 2010) on the theoretical PTE bound between two small antennas in the near-field region. The PTE is defined as the ratio of the power dissipated in the load of the receive antenna to the input power accepted by the transmit antenna:

$$PTE = \frac{R_{load}|I_2|^2 / 2}{R_{in}|I_1|^2 / 2} \tag{1}$$

where R_{load} is the load resistance, I_2 is the current at the load of the receiving antenna, R_{in} is the input resistance and I_1 is the current at the feed point of the transmitting antenna. To derive the maximum possible PTE for small antennas, (Lee & Nam 2010) assumed that the

field radiated by a small electric dipole antenna can be expressed in terms of the TM_{10} spherical harmonic. Using the addition theorem of spherical wave functions, the radiated field from the transmit antenna can be re-expressed in terms of impinging spherical modes on the receive antenna. The strength of the resulting inward-traveling TM_{10} mode onto the receive antenna can thus be found. From this field-based formulation, a two-port description of the transmit-receive antenna system is obtained. Next, they assumed that the optimal load to achieve maximum power transfer, or the so-called Linville load (Balanis, 1997), is used on the receive antenna. The final maximum PTE bound takes on the following simple, closed-form expression:

$$PTE = \frac{|T|^2}{2 - \mathrm{Re}\left[T^2\right] + \sqrt{4\left(1 - \mathrm{Re}\left[T^2\right]\right) - \mathrm{Im}\left[T^2\right]^2}}$$
$$T = \eta\frac{3}{2}\cdot\left[-\sin^2\theta\frac{1}{jkd} + \left(3\cos^2\theta - 1\right)\cdot\left\{\frac{1}{(jkd)^2} + \frac{1}{(jkd)^3}\right\}\right]\cdot e^{-jkd} \quad (2)$$

In the above expression, η is the radiation efficiency of the receiving antenna, θ is the angle of the receiving antenna with respect to the transmitting antenna (see inset to Fig. 2), $k=2\pi/\lambda$ is the free-space wave number and d is the spacing between the antennas. The same bound also holds true for a small magnetic dipole, or a small loop antenna, as the excitation of the TE_{10} mode leads to the same final expression.

The PTE bounds vs. distance (measured in wavelengths) are computed using (2) and plotted in Fig. 2 for different η and θ values. It is observed that higher PTE is achieved when the two antennas are in the co-linear configuration ($\theta=0$) than when they are in the parallel configuration ($\theta=\lambda/2$) up to a distance of 0.4λ. This is clearly a feature unique to the near-field region. Beyond this distance, our usual far-field intuition takes hold, i.e., antennas couple much more strongly in the parallel instead of the co-linear configuration. Several additional antenna design implications can be inferred from Fig. 2. First, we observe that PTE decreases rapidly as η decreases, implying that antennas with high radiation efficiency are needed to achieve the best results. It is crucial that any dissipative losses in the antenna are small relative to the radiated power. For example, simply using very short dipoles will not be a good choice to realize efficient power transfer since they have small radiation resistance and thus poor radiation efficiency when constructed using real conductors. Another important consideration is impedance matching. The PTE bounds in Fig. 2 are derived by assuming a different optimal load value is used at every distance. Any deviation from this optimal load will critically lower the realizable PTE. In the far field, the optimal load is simply the conjugate of the input impedance of the receiving antenna. In the coupled mode region, this conjugate matching condition is strongly violated. Fortunately, the conjugate matching condition is only weakly perturbed in the near-field region, since the antennas are not strongly coupled. Therefore, enforcing the conjugate matching condition leads to a good design choice for power transfer in the near field, without the need for a complex matching network that is a function of antenna separation. If a 50Ω load is desirable from a practical point of view, the receiving antenna can be designed to have an input impedance of 50Ω to approach the PTE bound. The same antenna design, when used for the transmit antenna, will also present a convenient impedance for the transmitter circuitry.

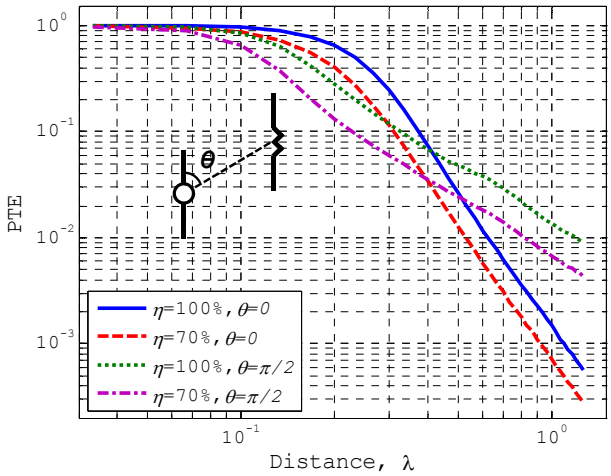

Fig. 2. PTE bound versus distance for different radiation efficiencies and antenna orientations. ©2010 IEEE (Yoon & Ling, 2010).

2.2 Design of electrically small, folded cylindrical helix (FCH) antennas

To approach the theoretical PTE bound using electrically small antennas, we need to design highly efficient antennas with a 50Ω input impedance. As discussed in Sec. 1, the folded cylindrical helix (FCH) is one such candidate with a good form factor and a well-understood design methodology. Since the radiation resistance of an electrically small antenna drops quadratically as a function of its height, the FCH design uses the folding concept to step up the small radiation resistance to improve the radiation efficiency and provide good matching. When N multiple folding arms are used for a highly symmetrical antenna structure, equal currents are induced on all the arms, resulting in a radiation resistance (R_{rad}) that scales approximately as N^2 while the loss resistance (R_{loss}) is increased only by a factor of N, thus leading to a high radiation efficiency (Lim & Ling, 2006).

Fig. 3 shows the designed FCH dipole operating at 200MHz based on 18-gauge copper wires. The diameter and height of the antenna are chosen to be approximately equal and are confined to a maximum dimension of 10.5cm. The antenna fits within a kr=0.31 sphere. NEC is utilized in the antenna modeling. The number of turns (1.25-turn) and the number of arms (4 arms) are chosen to reach the input impedance target of 50Ω while achieving a resonant frequency of 200MHz. The resulting antenna has an input resistance of 48.9Ω with a corresponding η of 93% based on NEC simulation.

Two FCH dipoles based on the above design are built and tested. They are constructed by winding copper wires on paper support. During testing, the feed point for each FCH is connected to a 2:1 transformer balun, which is characterized separately. The balun is then de-embedded from the measurement to obtain the S_{11} of each antenna. Fig. 4 compares the simulated and measured input impedances. As can be seen in Fig. 4, the measured results are shifted slightly downward by 5MHz from the simulation. This is due to fact that the wire windings in the built antennas are slightly longer than the design. However, the input resistances are still measured to be 49.1Ω and 48.9Ω, respectively, at their resonant frequencies. This pair of antennas are used as the transmit and receive antennas in the PTE measurement.

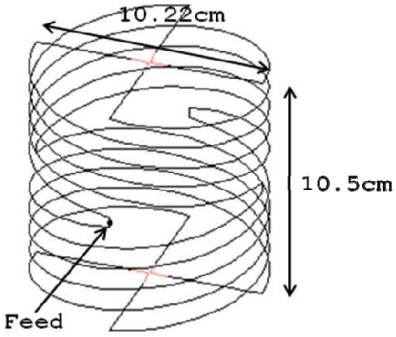

Fig. 3. The designed 1.25-turn, 4-arm folded cylindrical helix dipole. ©2010 IEEE (Yoon & Ling, 2010).

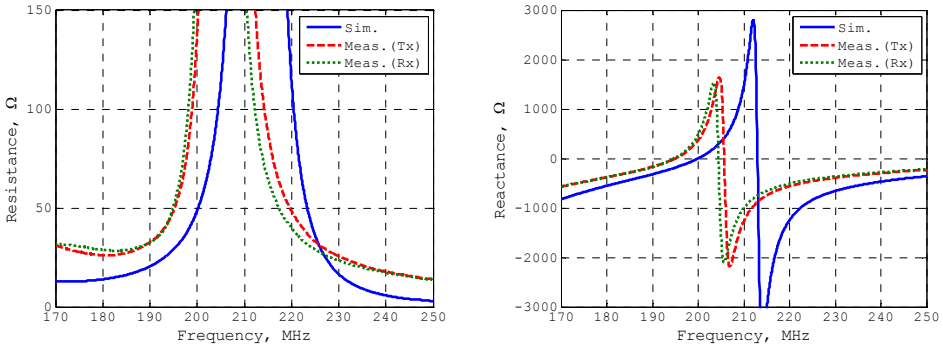

(a) (b)

Fig. 4. Simulated and measured input impedance of the folded cylindrical helix dipole. (a) Input resistance. (b) Input reactance. ©2010 IEEE (Yoon & Ling, 2010).

2.3 Near-field power transfer simulation and measurement

The power transfer efficiency between the two designed FCH antennas is simulated using NEC as well as measured. In the simulation, a 50-Ω resistive load is placed on the receive FCH. In this manner, any potential impedance mismatch between the receiver and the load is reflected in the resulting PTE value. The center-to-center distance between the two FCHs is varied from 0.15m to 2m. At very close-in range the resonant frequency of each antenna splits into two, which is consistent with the even and odd mode behavior in the coupled mode region (Kim & Ling, 2007). For the measurement, the FCH dipoles are mounted on 2m-high tripods and measured using a vector network analyzer. Fig. 5 shows the photos for the outdoor measurement setup. PTE is calculated from the measured S-parameters as $|S_{21}|^2/(1-|S_{11}|^2)$. The two baluns are again de-embedded to obtain the S_{21} between the two antennas. Both the co-linear and parallel configurations are simulated and measured.

(a) (b)

Fig. 5. Photos of the outdoor measurement setup. Each FCH is connected to a 2:1 transformer balun. (a) $\theta=0$. (b) $\theta=\pi/2$. ©2010 IEEE (Yoon & Ling, 2010).

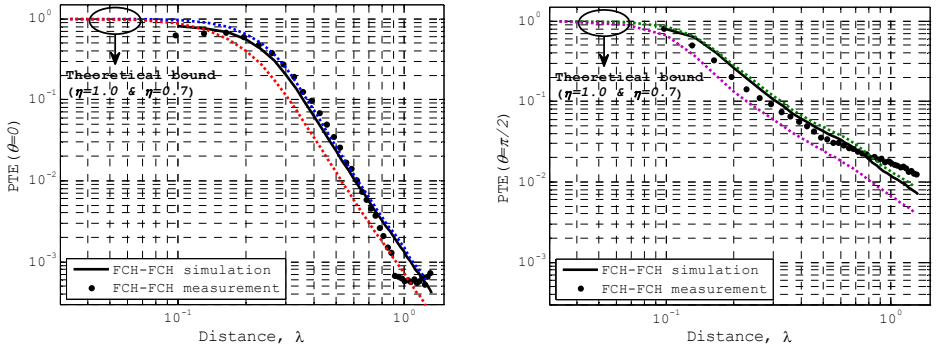

(a) (b)

Fig. 6. Simulated and measured PTE of two FCH-FCH dipoles. (a) $\theta=0$. (b) $\theta=\pi/2$. ©2010 IEEE (Yoon & Ling, 2010).

Fig. 6 shows the simulated (solid lines) and measured (dots) PTE results versus distance in wavelength. The PTE bounds from Eq. (2) shown earlier in Fig. 2 are re-plotted as dotted-lines for comparison. We observe that the simulated FCH-FCH results nearly approach the theoretical PTE bound with η=100%. The minor difference between them can be attributed to the slightly less than ideal radiation efficiency of the real FCH antenna (η=93%) and the small mismatch between the receive antenna and the load. We also observe from Fig. 6a that the simulated PTE curve begins to deviate more from the η=100% reference when the two antennas are very close to each other. This deviation is due to the increasing difference between the optimal Linville load Z_{Linv} and the resistive 50Ω load when the antennas begin to couple tightly at closer distances. The measured FCH-FCH results (shown as dots in both Figs. 6a and 6b) follow the simulation results fairly well. The discrepancy is likely caused by the non-negligible physical size of the balun boxes and the slight misalignment during the measurement. Overall, the measurement results clearly demonstrate that practical electrically

small antennas can be designed and realized to approach the theoretical bounds derived in (Lee & Nam, 2010) for wireless power transfer beyond the coupled mode region. The measured results showed a PTE of 40% at a distance of 0.25λ in the co-linear configuration, very close to the theoretical bound. For comparison, the meander monopole antennas reported in (Kim & Ling, 2007) showed a 40% PTE at a much shorter distance of 0.044λ (0.31m at 43MHz) in the parallel configuration. This section highlights the role of the theoretical bound in guiding antenna design. It also underscores the importance of antenna design in achieving highly efficient power transfer in the near field. In the next two sections, we explore possible ways to further extend the range or efficiency of the power transfer.

3. Power transfer enhancement using transmitter diversity and receiver diversity

One way to extend the range or efficiency of the power transfer in the near-field region is to use receiver and/or transmitter diversity (see Fig. 7). Multiple receiver scenarios have been studied in the coupled mode region to power multiple devices simultaneously from a single source (Cannon et al., 2009; Kurs et al., 2010). Multiple transmitting and receiving coils have also been investigated for device charging at very close range (Casanova et al, 2009). Here, we focus our attention on transmitter and receiver diversity in the near-field region.

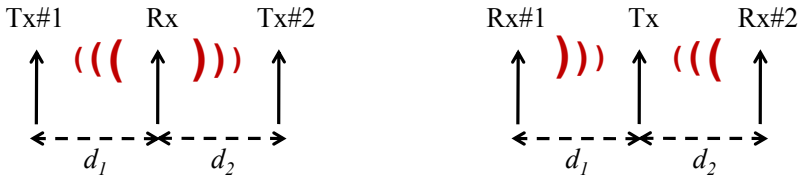

Fig. 7. Diversity configuration. (a) Transmitter diversity. (b) Receiver diversity.

3.1 Near-field power transfer bound under transmitter diversity

To begin, we define the PTE for multiple transmitters and a single receiver as the ratio of the power dissipated in the load to the total power accepted by the transmit antennas. For the two transmitter case, this is given as:

$$PTE = \frac{\mathrm{Re}\{Z_{load}\} \cdot |I_3|^2 / 2}{\mathrm{Re}\{V_1 \cdot I_1^*\} / 2 + \mathrm{Re}\{V_2 \cdot I_2^*\} / 2} \tag{3}$$

where Z_{load} is the load impedance, I_3 is the current at the load of the receiving antenna (port 3), V_1, V_2 are the input voltages and I_1, I_2 are the currents at the feed points of the transmitting antennas (ports 1 and 2). With specified input voltages at the transmitter ports and a given load, the terminal currents can be obtained once the 3-by-3 Z-matrix of the network is known:

$$\begin{bmatrix} Z_{11} & Z_{12} & Z_{13} \\ Z_{21} & Z_{22} & Z_{23} \\ Z_{31} & Z_{32} & Z_{33} \end{bmatrix} \begin{bmatrix} I_1 \\ I_2 \\ I_3 \end{bmatrix} = \begin{bmatrix} V_1 \\ V_2 \\ -I_3 \cdot Z_{load} \end{bmatrix} \tag{4}$$

To obtain the Z-matrix, we can extend the mutual impedance expression between two electrically small antennas derived by Lee and Nam (Lee & Nam, 2010) to the multiport case as follows:

$$Z_{mn} = \begin{cases} Z_a, & m = n \\ \mathrm{Re}[Z_a] \cdot T, & m \neq n \end{cases} \tag{5}$$

In Eq. (5), we approximate the self impedance by Z_a, the stand-alone impedance of a small dipole, which can be calculated using the induced EMF method (Balanis, 1997). T is described in Eq. (2). To compute the upper PTE bound, we need to find the optimal value for Z_{load}, Z_{opt}. Unfortunately, the closed form solution (i.e., the Linville load) used in Sec. 2 is only available for a two-port network. For three ports or more, a numerical optimization must be performed. Based upon (3) through (5), a local search for Z_{opt} to reach the maximum PTE is carried out with the antenna configuration shown in Fig. 7(a). The separation of the transmitters is fixed as D and a single receiver is moved between them. The antennas are in the parallel configuration ($\theta=\pi/2$) and the radiation efficiencies are set to 100%. To compute the bound, the optimal load is found numerically at every receiver position, with the conjugate value of the input impedance of the receiving antenna as the initial guess. The same input voltages are assumed ($V_1=V_2$) at the two transmitters. For Z_a, we use a value of 0.079-11270j [Ω], which is the input impedance for a λ/50 dipole computed by the induced EMF method.

Figs. 8a and 8b show the maximum PTE bounds derived in this manner when the transmitters are 0.7λ and 1.0λ apart, respectively. The theoretical PTE bound for the single transmitter case is also plotted by dashed lines for reference in both figures. In Fig. 8a, it is interesting to see that a very stable PTE region can be created as a function of the receiver position d. A PTE of 22% is maintained over a 0.2λ–0.5λ region between the two transmitters. This is also significantly improved from that of the single transmitter case. In this region, the fields due to the two transmitters add constructively since the receiver distance from the two transmitters is small. However, at larger spacing between the transmitters, rippling starts to appear due to the expected standing wave interference. This is shown in Fig. 8b for D=1.0λ.

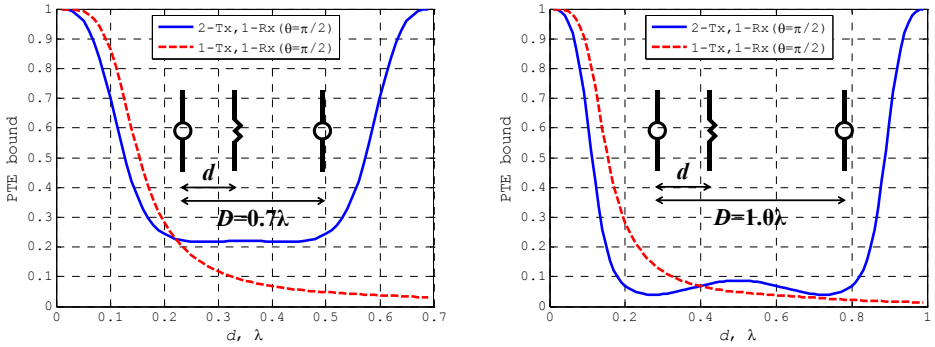

Fig. 8. PTE bound for transmitter diversity (two transmitters and one receiver) in the parallel configuration. The two transmitters are separated by the fixed distance D. (a) D=0.7λ. (b) D=1.0λ. ©2011 IEEE (Yoon & Ling, 2011).

To realize this PTE bound under transmitter diversity in practice, impedance matching and antenna radiation efficiency need to be addressed. Z_{opt} for the PTE bound calculation in Fig. 8a (D=0.7λ) is plotted in Fig. 9. For reference, Z_a=0.079-11270j [Ω]. It is observed that Z_{opt} is also rather stable in the flat PTE region of 0.2λ–0.5λ. In particular, its numerical value is close to the conjugate of the input impedance of the stand-alone antenna. An important implication of this observation is that if we want to use a constant 50-Ω load, then it is acceptable to design the receiving antenna to have an input impedance of 50Ω to approach the upper PTE bound in the region. In terms of radiation efficiency of the antennas, it is observed from simulation that the PTE decreases significantly as the radiation efficiency is reduced. This is the same as the conclusion reached earlier in Sec. 2. Therefore, the antennas should be designed to have radiation efficiency as close to 100% as possible.

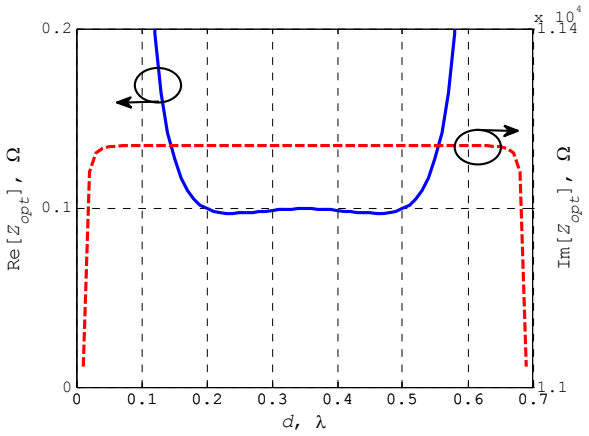

Fig. 9. Optimal load value (Z_{opt}) for the PTE bound with 0.7λ separation between the transmitters (Fig. 8a case), with respect to Z_a=0.079-11270j [Ω]. ©2011 IEEE (Yoon & Ling, 2011).

3.2 Power transfer simulation and measurement

We set out to demonstrate through simulation and measurement that the derived PTE bound can be approached using actual antennas. The same electrically small FCH dipoles designed in Sec. 2 are used. The antenna has an input resistance of 48.9Ω with a corresponding radiation efficiency of 93% and fits inside a kr=0.31 sphere at 200MHz. Three identical FCH dipoles are used in the NEC simulation and the setup is shown in Fig. 10. Two FCH dipoles are used as transmitting antennas with a separation of 1.05m (0.7λ at 200MHz, as measured between the two antenna ports), and an FCH dipole with a fixed 50-Ω resistive load is used as the receiving antenna. The position of the receiving antenna is changed between the transmitters from 0.15m to 0.90m. PTE is calculated using Eq. (3) at a fixed frequency of 200MHz.

For measurement, three FCH dipoles are first fabricated and measured. They are tuned to have the same resonance frequency. The measured input resistances of the three antennas are 61.7 Ω, 63.5 Ω and 55.3 Ω at 194.5 MHz. During the PTE measurement, the three FCH dipoles are mounted on 2m high tripods to minimize ground effects and measured using a vector network analyzer. The two transmitting FCH dipoles are separated by 1.08m (0.7λ at

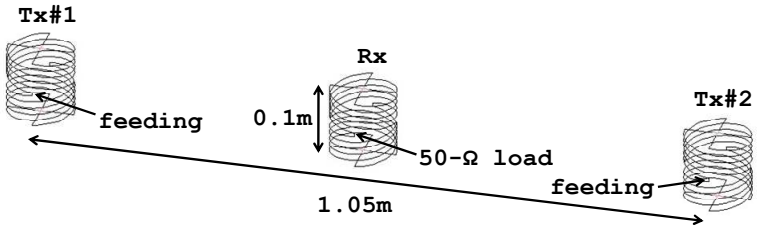

Fig. 10. NEC simulation setup for the two-transmitter and one-receiver scheme using electrically small folded cylindrical helix dipoles. The antennas are in the parallel configuration. ©2011 IEEE (Yoon & Ling, 2011).

194.5MHz) and the receiving one is moved from 0.15m to 0.90m. The 3-by-3 scattering matrix of the antennas at each position is obtained by three sets of measurements. In each set, one antenna is terminated by a 50-Ω load while the other two are connected through the baluns to the ports of the vector network analyzer. The baluns are characterized and de-embedded to obtain the S-parameters. The PTE is calculated from the measured S-parameters as:

$$PTE_{meas} = \frac{|S_{31}+S_{32}|^2}{1-|S_{11}+S_{12}|^2+1-|S_{22}+S_{21}|^2} \tag{6}$$

where ports 1 and 2 are for the transmit antennas and port 3 is for the receive antenna.
The simulated and measured PTE (D=0.7λ) versus the position of the receiving antenna is shown in Fig. 11. The derived theoretical PTE bound is re-plotted as a solid line for reference. The simulated PTE values using the FCH dipoles are plotted as red circles. They approach the theoretical PTE bound between 0.2λ and 0.5λ, showing a stable 20% PTE region. The slightly lower PTE from the theoretical bound is due to the imperfect radiation efficiency of the designed FCH dipoles and a small load mismatch. It is interesting to see

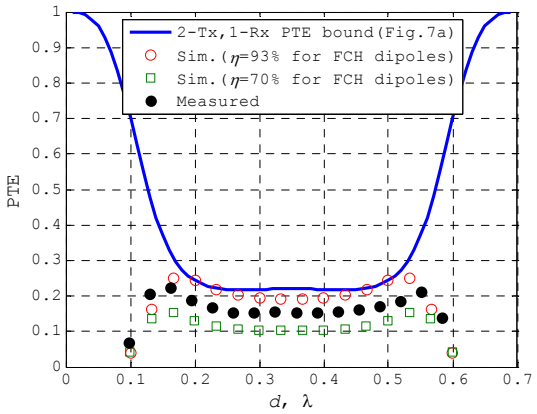

Fig. 11. Simulated and measured PTE for transmitter diversity using three FCH dipoles. ©2011 IEEE (Yoon & Ling, 2011).

that the PTE drops sharply as the receiving FCH dipole moves close to each transmitting antenna (i.e. the regions d<0.2λ and d>0.5λ). This phenomenon can be explained by the large load mismatch. Fig. 9 shows that the real part of the optimal load value deviates from the center region due to strong coupling as the receiving antenna comes close to either transmitter. The measurement result is plotted as black dots and it follows the trend of the simulation, showing the same stable PTE region. However, the PTE level is about 3% lower than the simulation. To explain this difference, the PTE is simulated using the same FCH dipoles but their radiation efficiency is lowered to 70%. It shows an even lower PTE level than the measurement. A Wheeler cap measurement is also performed for the fabricated FCH dipoles and the measured radiation efficiencies are between 80% and 90%. Therefore, we conclude that the lower radiation efficiencies of the built antennas are the main cause of the lower PTE values as compared to the simulation. This again highlights the importance of high antenna efficiency for achieving efficient near-field power transfer.

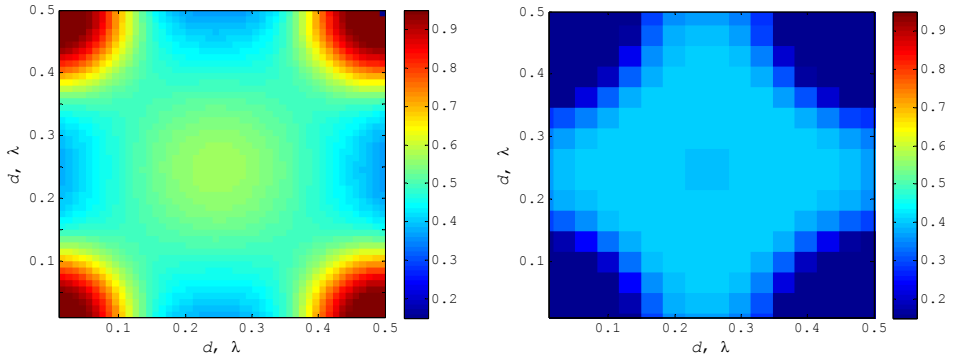

Fig. 12. Four-transmitter and one-receiver scheme. (a) PTE bound. (b) NEC simulation using electrically small folded cylindrical helix dipoles. ©2011 IEEE (Yoon & Ling, 2011).

Finally, the two-transmitter and single-receiver case is extended to four transmitters and a single receiver over a two-dimensional region. The same method used for the two transmitter case is used for the PTE derivation except that a 5-port network is considered. The four transmitters are located at the corners of a square region. The length of the diagonal region is set to 0.7λ and a single receiver is moved within the region. Again the optimal load for maximum power transfer is found through a numerical search. The derived PTE bound is plotted as a two-dimensional intensity plot in Fig. 12a. It is seen that a stable PTE of 50% is generated within a region of size 0.3λ at the center. Next, actual FCH dipoles are used in the PTE calculation. The optimal load value at each position is also replaced by a fixed 50-Ω load at the receive FCH dipole and the result is shown in Fig. 12b. The same trends as the two transmitter case are observed. First, when the receiver comes closer to each transmitter, the PTE again falls sharply due to load mismatch. Second, despite the slightly lower value (41%) from the PTE bound due to the imperfect radiation efficiency and load mismatch, the stable PTE region is created along the center region. Thus transmitter diversity can potentially be applied to provide a stable service region for one (or more) mobile receiver(s).

3.3 Near-field power transfer under receiver diversity

The PTE bound for receiver diversity can also be derived by using the same approach for the transmitter diversity. For two receivers, only the PTE definition is different and is given as:

$$PTE = \frac{\mathrm{Re}\{Z_{load,2}\} \cdot |I_2|^2 / 2 + \mathrm{Re}\{Z_{load,3}\} \cdot |I_3|^2 / 2}{\mathrm{Re}\{V_1 \cdot I_1^*\} / 2} \tag{7}$$

where port 1 is the transmitter and ports 2 and 3 are the receivers. $Z_{load,2}$ and $Z_{load,3}$ are the load impedances.

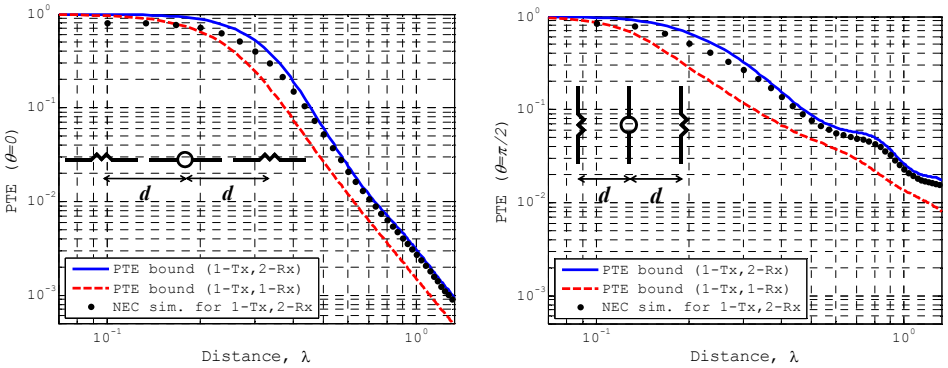

Fig. 13. PTE bound and NEC simulation result for receiver diversity (1-Tx, 2-Rx). (a) $\theta=0$. (b) $\theta=\pi/2$.

Fig. 13 shows the PTE bounds for the co-linear and parallel configurations. In these plots, the distances between the transmitter and the two receivers are set to be equal to simplify the calculation. The result of this constraint is that the optimal load impedances at the two receiving antennas are the same, thus simplifying the numerical search. The efficiencies of the antennas are set as 100%. The PTE bounds for the single transmitter and single receiver case are plotted in dashed lines for reference. As expected, the PTE bound is extended under receiver diversity. However, some rippling of the PTE curve can be seen due to coupling of the antennas. NEC simulation using three FCH dipoles (R_{in}=48.9Ω, η=93% and kr=0.31) with fixed 50-Ω loads is also carried out and the result is plotted as dots in Fig. 13. Not surprisingly, it follows the PTE bound well as it did in the single-transmitter single-receiver scenario.

In this section, we have derived the upper bounds for power transfer under the transmitter diversity and receiver diversity scenarios. It was also shown that such bounds can be approached by using highly efficient electrically small antennas. Generalization to the case of multiple transmitters and multiple receivers is reported in (Jun, 2011).

4. Power transfer enhancement using small directive antennas

Another possible way to enhance the range or efficiency of near-field wireless power transfer is to use spatial focusing antennas. While the role of directivity is very clearly described by the Friis transmission formula in the far field, spatial focusing in the near field

is not as well understood (Schantz, 2005; Kim et al., 2010). In the derivation of the upper bound for near-field power transfer in (Lee & Nam, 2010), only the lowest TM_{10} or TE_{10} mode was considered. In this section, we investigate whether small directive antennas can be used as a means of increasing the range or PTE of near-field power transfer.

4.1 Feasibility and antenna design considerations

We first test the feasibility of near-field coupling enhancement using directive antennas designed for far-field application. Uzkov showed that the end-fire directivity of a periodic linear array of N isotropic radiators can approach N^2 as the spacing between elements decreases, provided the magnitude and phase of the input excitations are properly chosen (Uzkov, 1946). Such a directivity value represents the so-called "superdirectivity" when compared to the maximum attainable directivity for isotropic elements spaced half-wavelength apart, especially because the directivity increases as the length of the linear array becomes smaller (Altshuler et al., 2005). Thus, the directivity of a two-element array of isotropic radiators would approach a value of four, i.e., 6 dB higher than that of a single isotropic radiator. Parasitic implementation of superdirectivity is also feasible. For example, a two-element, 0.02λ spacing Yagi antenna with a driver and a reflector each about half-wavelength (driver: 0.4781λ and reflector: 0.49λ) shows a directivity of 7.2dB in the far field (Lim & Ling, 2006). This configuration is chosen for both the transmit and receive antennas in our near-field PTE simulation. Under no conductor losses and with the optimal load (Z_{Linv}) for maximum coupling at every distance, the PTE between two such antennas is calculated. We shall call this particular antenna configuration under no conductor loss and with the optimal load an "idealized superdirective array" in subsequent discussions.

The calculated PTE is shown by a solid line in Fig. 14. PTE enhancement is observed from 0.1λ as compared to the PTE bound derived for small antennas, which is plotted by a dashed line. At far distances, the enhancement approaches about 11 dB, which is well predicted by the Friis far-field formula (2*(7.2dB-1.76dB)). While the solid line in Fig. 14 shows an impressive improvement in PTE performance when directive antennas are used, there are practical implementation issues. First, when the optimal load is replaced by a fixed 50-Ω

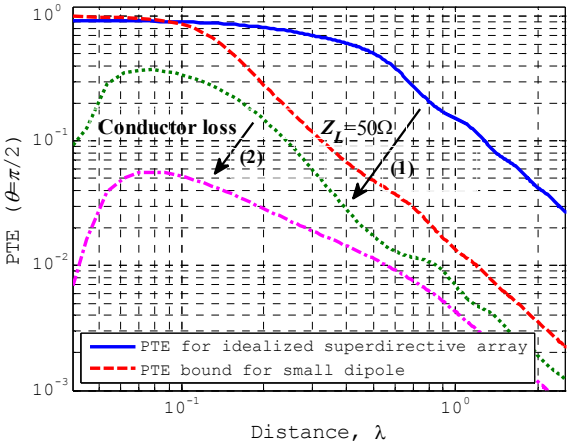

Fig. 14. PTE enhancement in the near-field region using an idealized superdirective array.

load, the PTE degrades sharply, as marked by the first arrow in Fig. 14. Second, the PTE degrades even more if conductor loss is considered, as marked by the second arrow in Fig. 14. These degradations are similar to the well-known pitfalls in realizing superdirective antennas for far-field applications, namely, an idealized superdirective array often comes with a large impedance mismatch and low radiation efficiency when implemented in practice. Therefore, to capture the benefit of high directivity for near-field power transfer, one must pay careful attention to antenna design. First, the radiation efficiency of the antenna should be high to minimize the conductor loss effect. Second, the input impedance of the antenna needs to be close to 50Ω for impedance matching to a standard 50-Ω resistive load. Finally, it is desirable that the antenna size be as small as possible.

4.2 Design of an electrically small FCH Yagi

We present in this section an electrically small Yagi antenna designed based on the FCH dipole to achieve good directivity, radiation efficiency and impedance matching. The antenna is comprised of two elements, a driver and a reflector. Each element is an FCH structure that has been thoroughly discussed in previous sections. The dimensions of the antenna including the height and the radius of each element, the spacing between the two elements and the number of arms are optimized using a local optimizer in conjunction with NEC. The far-field realized gain, which accounts for directivity, radiation efficiency and matching, is chosen to be the objective function.

The optimized antenna design and a photo of the fabricated antenna are shown in Fig. 15. The antenna feed is located at the center of one arm in the driver. The wire length of one arm in the driver is 85 cm (0.57λ at 200MHz) and that of the reflector is slightly longer at 92 cm (0.61λ at 200MHz). The entire antenna fits inside a kr=0.95 sphere, where r is the radius of the imaginary sphere that encloses the entire antenna. A copper wire radius of 0.5mm (18-AWG) is chosen for both elements. The optimized Yagi antenna has an input resistance of 50.9Ω at resonance with a corresponding radiation efficiency of 96%. The maximum simulated directivity, gain and realized gain in the forward direction at 200MHz are 6.76, 6.61 and 6.60dB, respectively. The front-to-back ratio is 12.3dB.

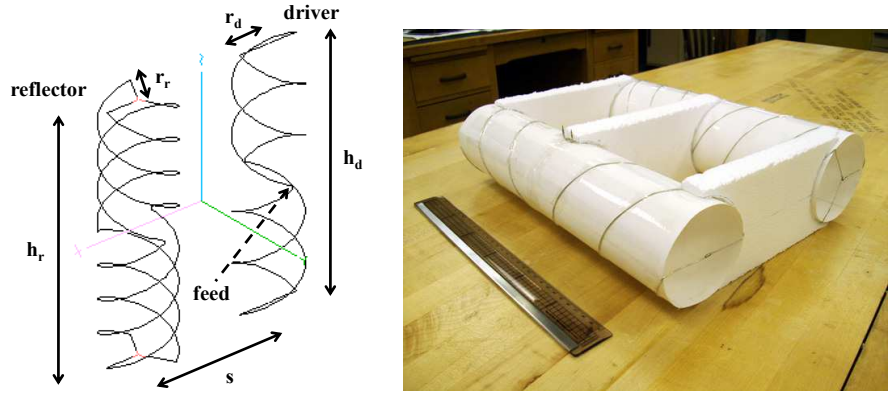

Fig. 15. Small FCH Yagi design. (a) NEC model: h_r=34.74; r_r=4.75; h_d=35.37; r_d=4.28; s=19.90 (units in centimeters); number of arms=three for reflector, two for driver; number of turns=1.25 for each arm. (b) Photo of the fabricated antenna. ©2011 Wiley (Yoon & Ling, 2011).

A prototype of the antenna in Fig. 15(a) is built by winding copper wires on paper support. The position of the reflector and driver parts is held in place by Styrofoam. The two small metal tips in the driver are connected to a 2:1 transformer balun in the measurement. The balun is characterized and de-embedded to obtain the S_{11} of the antenna. Fig. 16(a) shows the simulated and measured input impedances. Other than a slight downward shift of 5MHz, the measured results show good agreement with the simulation. The input resistance is measured as 56.0Ω at its resonant frequency of 195.3MHz. The simulated and measured realized gain and front-to-back ratio are plotted in Fig. 16(b). The measured realized gain is 6.2dB at 195.3MHz, which is lower than the simulated realized gain by 0.4dB. Minor RF interference noises can be observed at 175, 215, and 225MHz due to the outdoor environment. The front-to-back ratio is measured as 14.5dB at 195.3MHz, which is slightly higher than the simulated value of 12.3dB. The peaks above the resonant frequencies in both the measurement and simulation are due to a null in the backward direction.

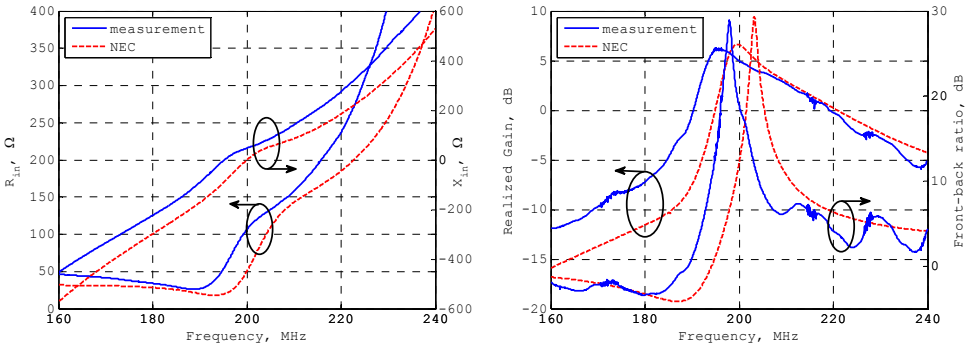

(a) (b)

Fig. 16. Simulation and measurement results from the designed FCH Yagi antenna. (a) Input impedance. (b) Realized gain and front-back ratio. ©2011 Wiley (Yoon & Ling, 2011).

4.3 Power transfer simulation and measurement

PTE values are simulated and measured using the two designed FCH Yagi antennas. A 50-Ω resistive load is placed on the receiving antenna in the NEC simulation. The distance between the antennas is measured as that between the centers of the two antennas. The photos for the outdoor measurement setup are shown in Fig. 17. The PTE is calculated from the measured S-parameters as $|S_{21}|^2/(1-|S_{11}|^2)$.

The simulated PTE results with the two FCH Yagi antennas with a fixed 50-Ω resistive load are shown as solid dots in Fig. 18. The PTE calculated with the idealized superdirective array (i.e. without conductor loss and with optimal load at every distance) in Fig. 14 is re-plotted for reference. The dashed line is the Friis far-field formula with two 7.2dB antennas. It is observed that the simulated PTE between the FCH Yagis follows the trend of the idealized superdirective array for spacing greater than 0.3λ. The discrepancy between the two is mainly caused by the lower directivity and radiation efficiency of the designed antennas as compared to the idealized superdirective array. When the two Yagi antennas are spaced less than 0.3λ, the PTE between them is rather degraded. This is due to the strong coupling between the antennas, which causes the current distribution on each Yagi antenna

to deviate from its stand-alone design for high directivity. The measured results are plotted as open circles and they show reasonable agreement with the simulation. Both the simulation and measurement show that 40% PTE is achieved at a distance of 0.45λ based on the center-to-center distance definition.

(a) (b)

Fig. 17. Measurement setup. (a) FCH Yagi-FCH Yagi. (b) FCH Yagi-FCH dipole.

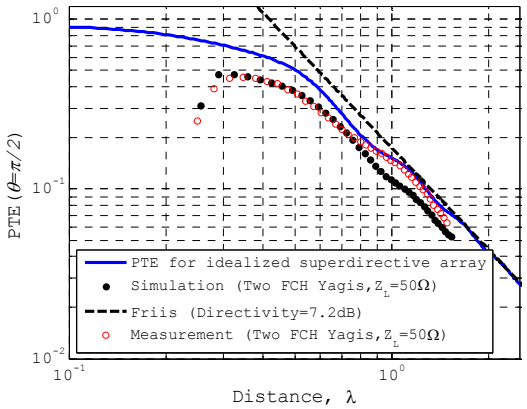

Fig. 18. Simulated and measured PTE for FCH Yagi-FCH Yagi.

To see the improvement in PTE by using directive antennas in the near-field region, the PTE results in Fig. 18 are compared to those from using FCH Yagi (Tx)-FCH dipole (Rx) and FCH dipole (Tx)-FCH dipole (Rx) in Fig. 19. The simulated values are plotted as lines and the corresponding measurement results are plotted as dots. At 0.45λ, the PTE difference between the FCH Yagi-FCH Yagi coupling and FCH dipole-FCH dipole coupling is 9.11 dB, showing good enhancement, though it is slightly lower than the 9.7 dB in the far field. This statement is also supported by the measurement results, which follow the simulation results fairly well. From this study, we see that the far-field realized gain can be used as a good surrogate for designing small directive antennas for near-field power transfer. This is an important practical consideration, since using PTE directly as the cost function is

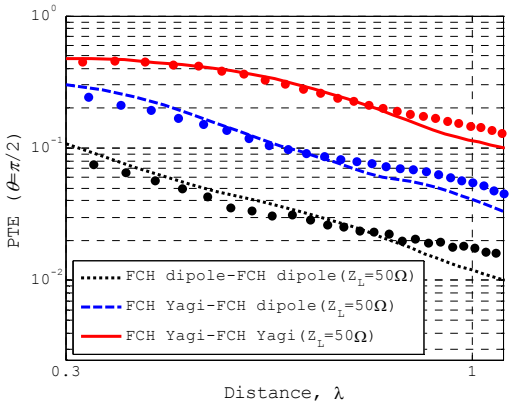

Fig. 19. PTE comparison. FCH dipole-FCH dipole, FCH Yagi-FCH dipole and FCH Yagi-FCH Yagi.

computationally more expensive and can lead to different designs at different distances. However, we also note that the PTE improvement comes at the price of antenna size, as the designed FCH Yagi has about a three-fold increase in *kr* as compared to that of the FCH dipole.

5. Conclusion

The use of the coupled mode resonance phenomenon for non-radiative wireless power is being studied intensively and many works have been reported. However, the distance over which such phenomenon exists is very short when measured in terms of wavelength. In this chapter, we have focused our attention on the near-field region beyond the coupled mode resonance region as a means of efficient wireless power transfer. First, the theoretical power transfer efficiency (PTE) bound was demonstrated by the design of electrically small, highly efficient folded cylindrical helix (FCH) dipole antennas. A 40% PTE was achieved at the distance of 0.25λ between the antennas in the co-linear configuration. To further extend the range or efficiency of the power transfer, transmitter diversity and receiver diversity were investigated. For transmitter diversity, it was found that a stable PTE region can be created when multiple transmitters are sufficiently closely spaced. Subsequently, such a stable PTE region was demonstrated using electrically small FCH dipoles. The measurement results highlighted the importance of maintaining high antenna radiation efficiency in realizing efficient wireless power transfer. For receiver diversity, it was found that the PTE can also be improved as the number of the receivers is increased. Finally, we investigated whether small directive antennas can be used as a means of enhancing near-field wireless power transfer. It was found that the range of efficiency can indeed be enhanced by using small directive antennas. It was also shown that the far-field realized gain is a good surrogate for designing small directive antennas for near-field power transfer.

To conclude this chapter, we shall mention several potential research topics that we believe are important for the practical implementation of near-field power transfer. First, the effects of surrounding environments on the near-field coupling should be carefully examined. One of the attractiveness of magnetic resonant coupling is that dielectric materials have only a

marginal effect on such mode of power transfer. We expect stronger material effects in the near field due to the presence of both electric and magnetic fields around self-resonant antennas. The interactions of the near fields with materials need to be quantified. Second, it would be interesting to study whether an optimal frequency exists for maximizing the range or efficiency of the transfer. 200MHz was chosen for all of the examples in this chapter as a matter of convenience in our measurements. A lower frequency would naturally lead to a longer absolute range in the power transfer. However, maintaining high efficiency in electrically even smaller antennas also becomes more challenging. Therefore, an optimal frequency may exist by considering the different practical implementation constraints (e.g., wire radius, antenna size). Some work has recently been reported along this line in (Poon et al., 2010). Finally, the design of orientation independent antennas is another topic that would be of interest in servicing mobile users.

6. References

Altshuler, E. E.; O'Donnell, T. H., Yaghjian, A. D. & Best, S. R. (Aug. 2005). A monopole superdirective array, *IEEE Trans. Antennas Propag.*, vol. 53, no. 8, pp. 2653–2661

Balanis, C. A. (1997). *Antenna Theory: Analysis and Design*, 2nd ed., John Wiley & Sons

Best, S. (Apr. 2004). The radiation properties of electrically small folded spherical helix antennas, *IEEE Trans. Antennas Propag.*, vol. 52, no. 4, pp. 953–960

Best, S. (Mar. 2009). A comparison of the cylindrical folded helix Q to the Gustafsson limit, in *Proc. EuCAP*, Berlin, Germany, pp. 2554–2557

Best, S. (Dec. 2009). The quality factor of the folded cylindrical helix, *Radioengineering*, vol. 18, pp. 343–347

Brown, W. C. (Sep. 1984). The history of power transmission by radio waves, *IEEE Trans. Microw. Theory Tech.*, vol. 32, pp. 1230–1242

Brown, W. C. (Jun. 1992). Beamed microwave power transmission and its application to space, *IEEE Trans. Microw. Theory Tech.*, vol. 40, pp. 1239–1250

Bolomey, J. C.; Capdevila, S., Jofre, L. & Romue, J. (2010). Electromagnetic modeling of RFID-modulated scattering mechanism. Application to tag performance evaluation, *Proc. IEEE*, vol. 98, no. 9, pp. 1555-1569

Cannon, B. L.; Hoburg, J. F., Stancil, D. D. & Goldstein, S. C. (Jul. 2009). Magnetic resonant coupling as a potential means for wireless power transfer to multiple small receivers, *IEEE Trans. Power Electronics*, vol. 27, pp. 1819–1825

Casanova, J. J.; Low, Z. N. & Lin, J. (Aug. 2009). A loosely coupled planar wireless power system for multiple receivers, *IEEE Trans. Industrial Electronics*, vol. 56, pp. 3060–3068

Choo, H and Ling, H. (Oct. 2003). Design of electrically small planar antennas using an inductively coupled feed, *Elect. Lett.*, vol. 39, pp. 1563-1564

Conner, M. (July 5, 2007). Wireless power transmission: no strings attached, *Electronic Design News*

Dobbins, J. A. & Rogers, R. L. (Dec. 2001). Folded conical helix antenna, *IEEE Trans. Antennas Propag.*, vol. 49, no. 12, pp. 1777–1781

Eom, K. & Arai, H. (Mar. 2009). Wireless power transfer using sheet-like waveguide, in *Proc. EuCAP*, Berlin, Germany, pp. 3038–3041

Finkenzeller, K. (2003). *RFID Handbook: Fundamentals and Applications in Contactless Smart Cards and Identification*, 2nd ed. Chichester, England; Hoboken, N.J.: Wiley

Fotopoulou, K. & Flynn, B. W. (Oct. 2006). Wireless powering of implanted sensors using RF inductive coupling, in *Proc. IEEE Conf. Sensors*, Daegu, Korea, pp. 765–768

Fotopoulou, K. & Flynn, B. W. (Mar. 2007). Optimum antenna coil structure for inductive powering of passive RFID tags, *in Proc. IEEE Intl. Conf. on RFID*, pp. 71–77, Grapevine, TX

Fotopoulou, K. & Flynn, B. W. (Feb. 2011). Wireless power transfer in loosely coupled links: coil misalignment model, *IEEE Trans. Magn.*, vol. 47, no. 2, pp. 416–430

Glaser, P. E. (1968). Power from the sun: its future, *Science*, vol. 162, pp. 857-886

Goubau, G. (1970). Microwave power transmission from an orbiting solar power station, *J. Microw. Power*, vol. 5, pp. 223–231

Hansen, J. E. (1988). Spherical near-field antenna measurements, *IEE Electromagnetic Waves Series 26*

Imura, T.; Okabe, H. & Hori, Y. (Sep. 2009). Basic experimental study on helical antennas of wireless power transfer for Electric Vehicles by using magnetic resonant couplings, in *Proc. IEEE VPPC*, Dearborn, MI, pp. 936–940

Jing, H. C. & Wang, Y. E. (Jul. 2008). Capacity performance of an inductively coupled near field communication system, in *IEEE Antennas Propag. Int. Symp. Dig.*, San Diego, CA

Johnston, R. H. & Haslett, J. W. (Jul. 2005). Antennas for RF mote communications, in *IEEE Antennas Propag. Int. Symp. Dig.*, Washington, DC, vol. 4A, pp. 267–270

Jun, B. W. (May 2011). An investigation on transmitter and receiver diversity for wireless power transfer, *MS thesis*, Univ. of Texas at Austin

Jung, Y.-K. & Lee, B. (Jul. 2010). Metamaterial-inspired loop antennas for wireless power transmission, in *IEEE Antennas Propag. Int. Symp. Dig.*, Toronto, ON, Canada

Kim, I.; Xu, S., Schmidt, C. & Rahmat-Samii, Y. (Jul. 2010). On the application of the Friis formula: simulations and measurements, in *Proc. URSI Nat. Radio Sci. Meeting*, Toronto, ON

Kim, Y. & Ling, H. (Nov. 2007). Investigation of coupled mode behavior of electrically small meander antennas, *IET Electronics Letters*, vol. 43, pp. 1250–1252Kim, Y. & Ling, H. (Jul. 2008). On the coupled mode behavior of electrically small antennas, in *Proc. URSI Nat. Radio Sci. Meeting*, San Diego, CA

Kurs, A.; Karalis, A., Moffatt, R., Joannopoulous, J. D., Fisher, P. & Soljacic, M. (Jun. 2007). Wireless power transfer via strongly coupled magnetic resonances, *Sciencexpress*, vol. 317, pp. 83–86

Kurs, A.; Moffatt, R. & Soljacic, M. (Jan. 2010). Simultaneous mid-range power transfer to multiple devices, *App. Phys. Lett.*, vol. 96, pp. 044102-1–044102-3

Lee, J. & Nam, S. (Nov. 2010). Fundamental aspects of near-field coupling small antennas for wireless power transfer, *IEEE Trans. Antennas Propag.*, vol. 58, no. 11, pp.3442–3449

Lim, S. & Ling, H. (Jul. 2006). Design of a thin, efficient, electrically small antenna using multiple folding, *Electron. Lett.*, vol. 42, pp. 895–896

Lim, S. & Ling, H. (2006). Design of a closely spaced, folded Yagi antenna, *IEEE Antennas Wireless Propag. Lett.*, vol. 5, pp. 302–305

McSpadden, J. O.; Little, F. E., Duke, M. B. & Ignatiev, A. (Aug. 1996). An inspace wireless energy transmission experiment, *IECEC Energy Conversion Engineering Conference Proceedings*, vol. 1, pp. 468–473

Mickle, M. H.; Mi, M., Mats, L., Capelli, C. & Swift, H. (Feb. 2006). Powering autonomous cubic-millimeter devices, *IEEE Antennas Propagat. Mag.*, vol. 48, pp. 11-21

Nalos, E. J. (Mar. 1978). New developments in electromagnetic energy beaming, *Proc. IEEE*, vol. 55, pp. 276–289

Pan, S.; Jackson, D. R., Chen, J. & Tubel, P. (May 2009). Investigation of wireless power transfer for well-pipe applications, in *Proc. URSI Nat. Radio Sci. Meeting*, Charleston, SC

Poon, A. S. Y.; O'Driscoll, S. & Meng, T. H. (May 2010). Optimal frequency for wireless power transmission into dispersive tissue, *IEEE Trans. Antennas Propag.*, vol. 58, no. 5, pp. 1739–1750

RamRakhyani, A. K.; Mirabbasi, S. & Chiao, M. (Feb. 2011). Design and optimization of resonance-based efficient wireless power delivery systems for biomedical implants, *IEEE Trans. Biomed. Circuits Syst.*, vol. 5, no. 1, pp. 48–63

Sample, A. & Smith, J. R. (Jan. 2009). Experimental results with two wireless power transfer system, *in Proc. IEEE Radio and Wireless Symp.*, pp. 16-18, San Diego, CA

Schantz, H. G. (Jul. 2005). A near field propagation law & a novel fundamental limit to antenna gain versus size, in *IEEE Antennas Propag. Int. Symp. Dig.*, Washington, DC

Shinohara, N. & Matsumoto, H. (Mar. 1998). Experimental study of large rectenna array for microwave energy transmission, *IEEE Trans. Microwave Theory Techniques*, vol. 46, no. 3, pp. 261–267

Smith, S.; Tang, T. B., Terry, J. G., Stevenson, J. T. M., Flynn, B. W., Reekie, H. M., Murray, A. F., Gundlach, A. M., Renshaw, D., Dhillon, B., Ohtori, A., Inoue, Y. & Walton, A. J. (Oct. 2007). Development of a miniaturised drug delivery system with wireless power transfer and communication, *IET Nanobiotechnology*, vol. 1, no. 5, pp 80–86

Strassner, B. & Chang, K. (2002). A circularly polarized rectifying antenna array for wireless microwave power transmission with over 78% efficiency, *IEEE MTT-S International Microwave Symposium Digest*, pp.1535–1538

Tesla, N. (1914). Apparatus for transmitting electrical energy, U.S. Patent 1119732

Thomas, E. M.; Heebl, J. D. & Grbic, A. (Jul. 2010). Shielded loops for wireless non-radiative power transfer, in *IEEE Antennas Propag. Int. Symp. Dig.*, Toronto, ON, Canada

Uzkov, A. I. (1946). An approach to the problem of optimum directive antennae design," *Comptes Rendus (Doklady) de l'Academie des Sciences de l'URSS*, vol. 53, pp. 35–38

Yaghjian, A. D. (Jan. 1982). Efficient computation of antenna coupling and fields within the near-field region, *IEEE Trans. Antennas Propag.*, vol. 30, no. 1, pp. 113–128

Yates, D. C.; Holmes, A. S. & Burdett, A. J. (Jul. 2004). Optimal transmission frequency for ultralow-power short-range radio links, *IEEE Trans. Circuits Syst. I, Reg. Papers*, vol. 51, no. 7, pp. 1405–1413

Yoon, I.-J. & Ling, H. (2010). Realizing efficient wireless power transfer using small folded cylindrical helix dipoles, *IEEE Antennas Wireless Propag. Lett.*, vol. 9, pp. 846–849

Yoon, I.-J. & Ling, H. (2011). Investigation of near-field wireless power transfer under multiple transmitters, *IEEE Antennas Wireless Propag. Lett.*, vol. 10, pp. 662–665

Yoon, I.-J. & Ling, H. (Jun. 2011). An electrically small Yagi antenna with enhanced bandwidth characteristics using folded cylindrical helix dipoles, *Microwave Optical Tech. Lett.*, vol. 53, pp. 1231–1233

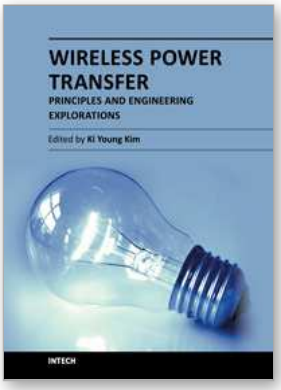

Wireless Power Transfer - Principles and Engineering Explorations
Edited by Dr. Ki Young Kim

ISBN 978-953-307-874-8
Hard cover, 272 pages
Publisher InTech
Published online 25, January, 2012
Published in print edition January, 2012

The title of this book, Wireless Power Transfer: Principles and Engineering Explorations, encompasses theory and engineering technology, which are of interest for diverse classes of wireless power transfer. This book is a collection of contemporary research and developments in the area of wireless power transfer technology. It consists of 13 chapters that focus on interesting topics of wireless power links, and several system issues in which analytical methodologies, numerical simulation techniques, measurement techniques and methods, and applicable examples are investigated.

InTech Europe
University Campus STeP Ri
Slavka Krautzeka 83/A
51000 Rijeka, Croatia
Phone: +385 (51) 770 447
Fax: +385 (51) 686 166
www.intechopen.com

InTech China
Unit 405, Office Block, Hotel Equatorial Shanghai
No.65, Yan An Road (West), Shanghai, 200040, China
中国上海市延安西路65号上海国际贵都大饭店办公楼405单元
Phone: +86-21-62489820
Fax: +86-21-62489821